The Alpehue geyser field, Sollipulli Volcano, Chile

Article · September 2020

CITATIONS
0

READS
197

7 authors, including:

Carolina Munoz Saez
Columbia University
21 PUBLICATIONS **234** CITATIONS
SEE PROFILE

Alonso Emilio Vargas Barrera
University of Chile
1 PUBLICATION **0** CITATIONS
SEE PROFILE

Martin Reich
University of Chile
171 PUBLICATIONS **3,859** CITATIONS
SEE PROFILE

M. Manga
University of California, Berkeley
551 PUBLICATIONS **15,744** CITATIONS
SEE PROFILE

Journal of Volcanology and Geothermal Research 406 (2020) 107065

Contents lists available at ScienceDirect

Journal of Volcanology and Geothermal Research

journal homepage: www.elsevier.com/locate/jvolgeores

The Alpehue geyser field, Sollipulli Volcano, Chile

Carolina Munoz-Saez [a,b,c,*], Carolina Perez-Nuñez [a,b], Sebastian Martini [d], Alonso Vargas-Barrera [a,b], Martin Reich [a,b], Diego Morata [a,b], Michael Manga [e]

[a] Department of Geology and Andean Geothermal Center of Excellence (CEGA), FCFM, Universidad de Chile, Santiago, Chile
[b] Millennium Nucleus for Metal Tracing Along Subduction, FCFM, Universidad de Chile, Santiago, Chile
[c] Lamont-Doherty Earth Observatory, Columbia University, Palisades, NY, USA
[d] Independent Consultant, Santiago, Chile
[e] Department of Earth and Planetary Science, University of California, Berkeley, CA, USA

ARTICLE INFO

Article history:
Received 8 August 2020
Received in revised form 17 September 2020
Accepted 18 September 2020
Available online 30 September 2020

Keywords:
Geyser
Silica sinter
Andes
Hydrothermal
Sollipulli

ABSTRACT

Natural geysers on Earth are uncommon and most of them are clustered in large basins that share common characteristics, specifically, a magmatic heat source, meteoric water supply, and a set of fractures and/or porous rocks that allow circulation, accumulation and periodic release of fluids. Most active geysers and sinter deposits in the Andes occur in the El Tatio geyser field (~10 km^2) in the Chilean Altiplano. Few of these features are reported in the southern volcanic zone. In this study, we characterized a small geyser field (with at least 4 geysers in ~0.2 km^2) called Alpehue located in southern Chile. This field is found in a steep canyon on a flank of Sollipulli Volcano. Besides geysers, the Alpehue field hosts several types of surface hydrothermal manifestations including perpetual spouters, sub-boiling hot springs, mud pools and sinter deposits. The different features occur in distinct geological units and are distributed at different topographic elevations. Geysers are restricted exclusively to a single lithological unit of highly hydrothermally altered breccia. The geochemical and δD-$\delta^{18}O$ isotopic compositions of thermal waters sampled from the geysers and perpetual spouters share a dominantly meteoric signature, and fluid-rock equilibration was inferred to have occurred in a deep reservoir >200 °C. This results in chloride-alkaline high silica waters that precipitate silica sinter at the surface. Radiocarbon ages of organic material contained within the sinter are up to at least 7.37 ± 0.02 ka CalBP. Micro-terraces (<3 cm) are the dominant texture of the sinter deposits with features that are controlled by the high topographic gradient. Our observations at Alpehue suggest that the high incision of the river enables the discharge of boiling water (rich in silica) at the surface. Precipitation of sinter at the surface, coupled with the high permeability of the breccia, creates a configuration that enables geysers to form and sustain episodic activity.

1. Introduction

Geysers are hot springs that episodically erupt boiling water, vapor, and non-condensable gases (e.g., White, 1967). While hot springs with continuous discharge are abundant on Earth's surface, natural geysers are uncommon. Fewer than 1000 active geysers have been described worldwide and >90% of them occur in large fields in Yellowstone National Park in the USA, Valley of Geysers in Russia, El Tatio in Chile, and Whakarewarewa in New Zealand (e.g., Hurwitz and Manga, 2017). These geyser fields have common characteristics: high heat flow mostly associated with Pleistocene magmatism; sufficient water, mainly from meteoric sources, into sustain the geyser eruptions and fractures and/or porous rocks to transmit and accumulate fluids (White, 1967; Kieffer, 1989; Ingebritsen and Rojstaczer, 1993, 1996; Kedar et al., 1998; Kiryukhin et al., 2012; Hurwitz and Manga, 2017; Munoz-Saez et al., 2015a, 2015b, 2016). Heat and water are common near volcanoes, but the underground geometry that allows the circulation, accumulation, and periodic release of fluids is unusual. A set of lateral fractures or cavities have been inferred from direct observations (Belousov et al., 2013; Walter et al., 2020) and seismic data (Vandemeulebrouck et al., 2013; Ardid et al., 2019; Wu et al., 2017), however, the structural and lithological controls leading to the right underground geometry to sustain geyser activity are still poorly constrained.

Thermal water erupted from geysers usually has a chloride-alkaline composition, near neutral pH, and high silica content (Fournier and Rowe, 1966; Weir et al., 1992). Cooling and evaporation of water around geysers and hot springs leads to the precipitation of silica, forming siliceous deposits called silica sinters. The term geyserite is used for near-vent sinter deposits characterized by finely laminated sinter with varied morphologies including nodular, spicular, botryoidal, and wavy stratiform micro-stromatolite-like structures (Campbell et al., 2015;

* Corresponding author at: Department of Geology and Andean Geothermal Center of Excellence (CEGA), FCFM, Universidad de Chile, Santiago, Chile.
E-mail address: caromuno@ing.uchile.cl (C. Munoz-Saez).

https://doi.org/10.1016/j.jvolgeores.2020.107065
0377-0273/

Hamilton et al., 2019a). Geyserite and other sinter deposits at the surface can provide a guide for exploring geothermal reservoirs and epithermal mineralization at depth, as they identify locations with subsurface structures that transported mineral-rich hot fluids (e.g. Fournier and Rowe, 1966; Simmons et al., 2005; Hamilton et al., 2018, 2019a, 2019b). Geysers are dynamic systems and sensitive probes of external perturbations, such as earthquakes and changes of water recharge (e.g., Rojstaczer et al., 2003; Husen et al., 2004; Hurwitz et al., 2008; Watts-Henwood et al., 2017; Campbell et al., 2019). Sinter deposits record the dynamic evolution of the hydrothermal system over geological time (e.g., Campbell et al., 2001, 2015; Guido et al., 2019; Slagter et al., 2019; Munoz-Saez et al., 2020). Sinter deposits also host and preserve microbial life, providing insights to early habitable environments on Earth and other planets (e.g., Farmer, 1998, 2000; Farmer and Des Marais, 1999; Westall et al., 2001; Konhauser et al., 2003).

Geysers and silica sinter deposits in the Andes have been reported mostly in the Central Volcanic Zone (CVZ) in Northern Chile, especially in the El Tatio geyser field that is the third largest geyser field in the world (Hurwitz and Manga, 2017; Munoz-Saez et al., 2018). However, in the Chilean Southern Volcanic Zone (SVZ), geysers are rare – to our knowledge, the only studies evidencing (local and limited) geyser activity were based in the Puyehue-Cordon Caulle volcanic system (Sepúlveda et al., 2004) and in the Tolhuaca geothermal system (extinct geyserite, Melosh et al., 2012).

In this study, we present geological and geochemical data to characterize a small geyser field, called Alpehue, located on the south east flank of the Sollipulli volcano in the SVZ of Chile (38°59′S - 71°30′W, Fig. 1). The Alpehue geysers are part of the Chilean geopark Kutralkura in the Araucanía Region of Chile (SERNAGEOMIN, 2019). In a recent assessment of geothermal feasibility in the region, Alpehue was described as the system of chloride thermal waters with the largest geothermal potential (Lemus and Honores, 2019). However, the area remains largely unexplored due limited access. Here, we aim to establish a relationship between the local geology and the development of geysers by mapping the distribution of the thermal vents and silica sinter deposits at Alpehue. Due to steep topography, we used an unmanned aerial vehicle (UAV) or "drone" to survey the field and complement our field observations of thermal manifestations and local geology. To determine the origin of the fluids, we analyzed the geochemical (major and minor ions) and isotopic (δD, $\delta^{18}O$) signature of the thermal and meteoric water. To better understand the dynamics of silica deposition, we analyzed the texture and composition of sinter deposits using scanning microscopy (SEM) and X-ray diffraction techniques. The field's longevity was estimated by dating two sinter samples near inactive vents using the radiocarbon (^{14}C) method. These data allow us to explore why geysers are so rare in the SVZ and to identify the combination of geological and geochemical characteristics that allow Alpehue to sustain geyser activity.

The primary objective of this study is to understand how the local geological environment enables geysers to form in a setting different from large geyser basins. We propose that a combination of factors including the river erosion, lithology, and the silica deposition can enable fluid discharge and geysering. Understanding these factors increases the potential of finding more of these small geothermal manifestations in the SVZ. Additionally, we aim to document the architecture of a high relief sinter deposit and its textures. Finally, we aim to improve the regional and local knowledge of the thermal fluids in the SVZ and their relationship to faulting and magmatism.

2. Geological setting

The Sollipulli Volcano is an active stratovolcano located in the Araucanía region of the Southern Andes Volcanic Zone (SVZ) in Chile, between the Llaima and Villarica volcanoes (Fig. 1). Sollipulli has an ice-filled, ~4 km diameter caldera located at an altitude of 2382 m above sea level (Hobbs, 2014). This current caldera overlies an older elliptical caldera of 5 × 4 km, with its axis elongated in the NE-SW direction. The volcanic edifice of the Sollipulli Volcano is bounded by two faults with strike close to NS, a segment of the Liquiñe-Ofqui fault system (LOFS) on the western flank, and the Reigolil-Pirihueico fault on the eastern flank (Fig. 1). Between these two main faults, a series of approximately NNE-striking volcanic structures and cracks have been described (Naranjo et al., 1993). The Sollipulli fault has been inferred to

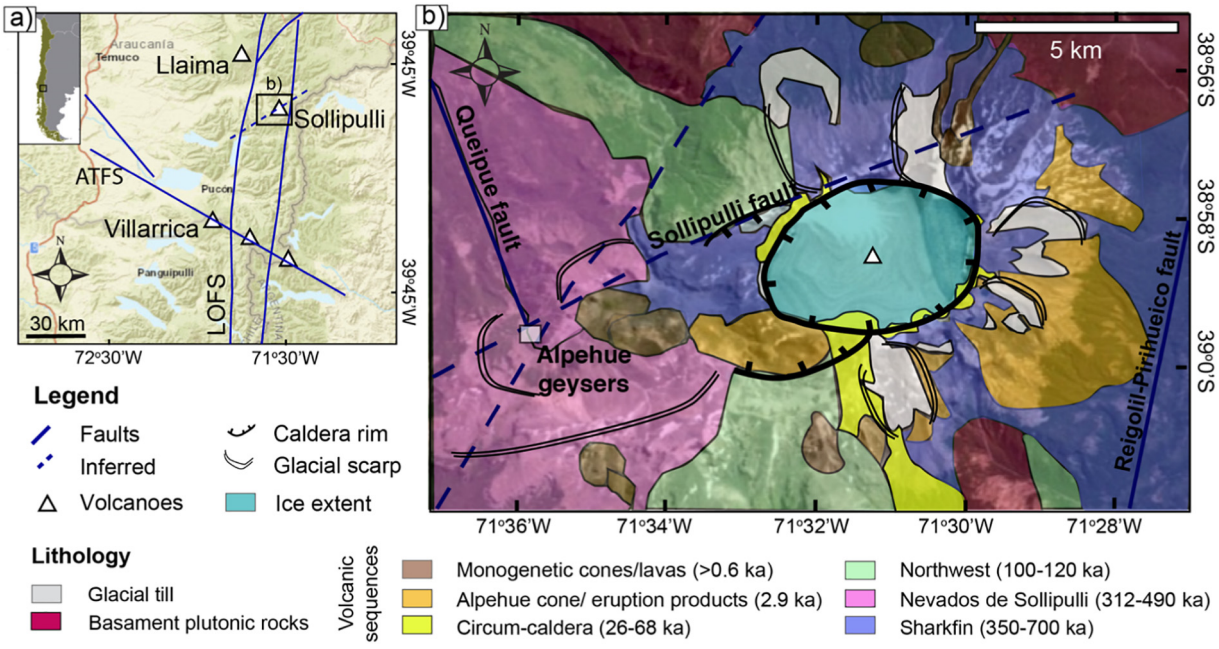

Fig. 1. (a) Regional context of Sollipulli area. The blue lines represent the main regional structural systems: the Liquiñe-Ofqui Fault System (LOFS) and the Andean Traverse Fault System (ATFS). (b) Local geological map of Sollipulli Volcano (the geology has been modified from Lachowycz et al., 2015; and the faults from Naranjo et al., 1993, López-Escobar et al., 1995, and Lemus and Honores, 2019). The eruption products of the Alpehue volcanic unit include ash falls, pyroclastic and lahar deposits. The Alpehue geyser field is located on the Nevados de Sollipulli volcanic unit. (For interpretation of the references to colour in this figure legend, the reader is referred to the web version of this article.)

follow the alignment of the main volcanic structures in a N70°E direction (López-Escobar et al., 1995).

Since the Pleistocene, the Sollipulli volcano has erupted magma with compositions ranging from basalt to trachydacite (Lachowycz et al., 2015). Earlier activity started with the Nevados de Sollipulli and Sharkin sequences, with ages >300 ka (Lachowycz et al., 2015) and basaltic to andesitic eruptions (Naranjo et al., 1993). The Alpehue Crater lies on the rim of the newer caldera, toward the southeast. This parasitic crater was formed after a large plinian eruption at 2.9 ka, generating ash falls, and pyroclastic and lahar deposits toward the northwest (Naranjo et al., 1993, Fig. 1). A series of small monogenetic cinder cones on the northeast flank of the volcano represent the most recent eruptions. One was documented to be ~700 years old, but the stratigraphic ages are poorly constrained (Naranjo et al., 1993).

Presently, two glacier outflow regions are recognized in the caldera, the Chufquén outflow in the north and the Alpehue outflow in the southwest (Fig. 1). Broad U-shaped valleys narrow into V shaped valleys dissecting the lava flows. Most of the lava flows on the volcano's flanks have glacial striations (Gilbert et al., 1996). Evidence of subglacial volcanic activity, including hyaloclastites, has been reported in the area (Gilbert et al., 1996; Murphy, 1996; Lachowycz et al., 2015). The Alpehue geothermal field is situated at the bottom of a glacial U-shaped valley, which has been further incised by the river. This site is located ~4.5 km from the Alpehue Crater on the southwest flank of the Sollipulli Volcano. The elevation of the field is ~1350 m a.s.l. and the boiling temperature at that elevation is ~95.4 °C. The supply of meteoric water in the region is dominated by seasonal rain and snow between April and September, with an average precipitation of 2.1 m/y (Tricauco station, DGA, 2020). Accessibility to the site is limited to the summer months between December and March, and the only access is by canyoneering up the river (Figs. 1, 2).

Preliminary data from the Alpehue hydrothermal field by Lemus and Honores (2019) indicate the predominance of boiling springs of silica-rich chloride-alkaline composition forming silica sinter deposits at the surface. This field is considered the main upflow from a geothermal reservoir with temperatures between 188 and 217 °C. Thermal manifestations lie on Pleistocene volcanic rocks of the Nevados de Sollipulli group. The hydrothermal field is located at the intersection of the NW-trending Queipue fault (Naranjo et al., 1993) and NE lineaments inferred to be faults (López-Escobar et al., 1995; Lemus and Honores, 2019). These faults are thought to permit the circulation of the fluids (Lemus and Honores, 2019).

3. Methodology

3.1. Field mapping and digital elevation model

We mapped the extent of the geyser field, hydrothermal deposits, the number of active vents, direction of the thermal water flow, and local lithology. The area explored is ~0.2 km^2. The geyser field is crossed by the Alpehue canyon, which runs approximately in the NE direction, creating a steep slope and limiting accessibility to the SE side of the canyon (Fig. 2a). By using an unmanned aerial vehicle (UAV) or "drone", we were able to map the NW side of the canyon and build the first digital elevation model (DEM) of the area (Fig. 2). We used a DJI Mavic Pro Platinum Quadcopter, which is equipped with a 12.71 MP camera; the flight was open planned and operated using a smartphone application called DroneDeploy. The software Agisoft Metashape Professional was used to reconstruct the 3D DEM in Fig. 2b. We flew at a speed of 3 m/s, an elevation of 63.6 m and we obtained images with a lateral and longitudinal overlap of 83%. The average size of the images was 4000 × 3000 pixels, and each image was automatically georeferenced with 3D coordinates from the UAV's global positioning system (GPS). We set 10 ground control points using a handheld GPS, which provided an accuracy up to 10 m on a clear day. The resulting DEM has an accuracy of 2.25 cm per pixel. By overlapping our field measurements on the DEM, we created 1:2000 scale geologic map (Fig. 2c).

3.2. Sinter characterization, microscopy and X-ray diffraction

Our study of the sinter deposits at Alpehue is mostly restricted to the area with geysers and perpetual spouters on the SE side of the river, due to the limited access to the mud pools and sub-boiling thermal springs near the channel (Fig. 2). We characterized 7 different sites on the more accessible SE side of the field and collected 22 sinter samples; additionally, one site close to the river was described (Fig. 2c). We define new or active sinters as those associated with active vents, while old sinters are associated with inactive vents or dry channels partially covered by grass. We classified the environment of formation according to distance from the vent and temperature (e.g., Lynne, 2012; Campbell et al., 2015; Hamilton et al., 2019a, 2019b). We defined proximal environments as those formed near vent with temperatures >65 °C, mid-temperature environments as those with temperatures between 45 and 65 °C, and distal environments as those with temperatures 20–45 °C. We studied the micro-textures of the silica sinter samples using a FEI Quanta 250 scanning electron microscope (SEM) at the Andean Geothermal Center of Excellence (CEGA), Department of Geology, Universidad de Chile in Santiago. We used an acceleration voltage of 15–20 kV and a focal distance of 10 mm. The structure and degree of crystallinity of the silica phases in 8 sinter samples were determined by using X-ray powder diffraction (XRD). The instrument used was a Bruker D8 Advanced Diffractometer, located in the Physics Department, Universidad de Chile, and the analytical conditions were: 2–80° 2θ in a rate of 0.02° in 0.2 s, at 40 kV, 30 mA, and CuKα of 15,604 Å.

3.3. Hydrogeochemistry and isotope composition

Temperature, pH, and electrical conductivity of the thermal waters were measured in situ in the field using a portable multiparameter meter and a FLIR camera. Due to the inaccessibility of some thermal sites, we focused on the area dominated by geysers and perpetual spouters, collecting 4 samples of thermal waters (Fig. 2c, perpetual spouters at sites 1,3,7 and the geyser at site 5). These sampling sites were colocated with those reported previously in Lemus and Honores (2019). This previous work also included the geochemistry of one mud pool of pH 3.8 and one spring on the river walls of neutral pH. For a more comprehensive interpretation of our data, we also considered the results by Lemus and Honores (2019).

In this study, major and trace element concentrations were measured at the Fluid Geochemistry Laboratory of CEGA, Department of Geology, Universidad de Chile. Anions were determined using ion chromatography (IC 861 Advanced Compact-Metrohm) and major cations were determined by atomic absorption spectrophotometry (AAS, Perkin-Elmer Pinaacle 900F). Carbonate abundance was obtained by volumetric titration methods following Giggenbach (1989). Concentrations of selected trace elements were analyzed using an inductively coupled plasma–mass spectrometer (ICP-MS) with collision cell (iCAP-Q, Thermo Scientific). All samples presented in this study have ionic balances of 95% or more, considering major elements and the most abundant trace elements. The isotopic measurement of hydrogen and oxygen in the samples was carried out using an isotope ratio mass spectrometer (IRMS) at the University of California, Berkeley, and expressed in delta notation (δD and $\delta^{18}O$, respectively). The water–CO_2 equilibration method was used for oxygen (Epstein and Mayeda, 1953) and the zinc-reduction method for deuterium (Coleman et al., 1982).

3.4. Radiocarbon dating

We collected two samples of old sinter deposits from inactive vents at sites 1 and 7 by hammering the surface of the rock outcrop. Sample

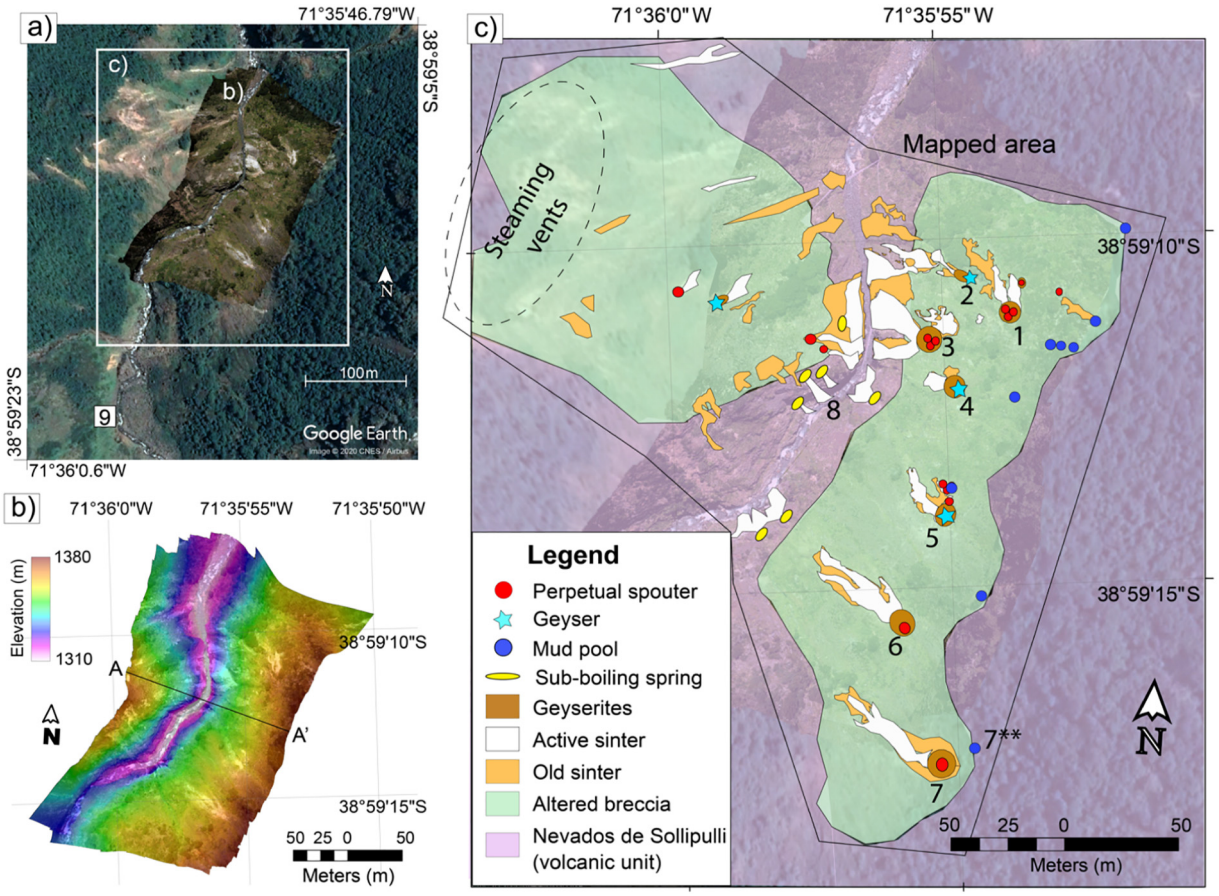

Fig. 2. (a) High resolution UAV aerial photometry overlain on a Google Earth view of the area. Site 9 corresponds to the sample of river water. (b) DEM of Alpehue canyon, (c) Geological map of Alpehue hydrothermal field indicating the position of type and position of the active vents, the distribution of sinters and the local lithology. The polygon indicates the area mapped in detail. Beyond this polygon the area was covered by trees, and we extrapolated the lithology of the volcanic unit described in the geological map Fig. 1b (Nevados de Sollipulli). The mapped altered breccia overlies the Nevados de Sollipulli volcanic unit.

preparation was carried out at the Fluid Geochemistry Laboratory of CEGA, Department of Geology, Universidad de Chile, following the methodology described in the recent literature (e.g., Howald et al., 2014; Lowenstern et al., 2016; Slagter et al., 2019; Munoz-Saez et al., 2020). Samples were soaked for 24 h in 1 M hydrochloric acid (HCl) to dissolve non-organic carbonates. Next, samples were immersed in concentrated (48%) hydrofluoric acid (HF) for 48 h. The sample from site 7 was large enough to obtain two aliquots. Finally, samples were combusted to CO_2, graphitized over an iron catalyst using the hydrogen reduction method (Vogel et al., 1984), and analyzed for ^{14}C using accelerator mass spectrometry at the at Keck-Carbon Cycle AMS facility, University of California, Irvine. A $\delta^{13}C$ value of −25‰ (Stuiver and Polach, 1977) was used to correct the measured ^{14}C activity for isotopic fractionation. All reported ages have been calibrated using the CALIB 7.1 code (Stuiver and Reimer, 1993), and the SHCal13 data set (Hogg et al., 2013) for the Southern Hemisphere.

4. Results

4.1. Lithology and distribution of active vents

On both sides of the river we found a hydrothermally altered volcaniclastic breccia at 1350 to 1370 m, filling the bottom of the glacial valley (Fig. 3a, c). The breccia is poorly sorted, matrix-supported, and with clasts up to 0.5 m of andesitic origin; however, we were not able to determine if its origin was alluvial or glacial. Vegetation distribution identifies the hydrothermal zone, with patches of grass growing over hydrothermally altered rocks and tall trees growing in non-altered areas. The active geysers, perpetual spouters, and sinter mounds are located on altered breccia (Fig. 3c, d), with an estimated thickness of ~10 to 20 m. Close to the upper limit of the hydrothermally altered breccia, below the tree line, at ~1370 to 1380 m elevation, we found mud pools with clay (Fig. 3e) and native sulfur deposits. Within the canyon, the river carved nearly vertical walls through highly fractured andesitic to basaltic volcanic rocks of the Nevados de Sollipulli volcanic group (Fig. 3f). Abundant thermal springs appear in the fractures, forming thin, millimeter-thick layers of sinter.

We characterized 4 active geysers, three of them on the SE side of the river (Fig. 2c): sites 2, 4 and 5. The site 2 has a vent of 0.4 m × 0.35 m that erupts a column of water and vapor up to 2.5 m high for 40 s every 30 to 40 min (Fig. 3d, Supplementary material: Video S1). The site 4 has a vent of 0.6 m diameter erupting a 1 m column of water for 90 s every 3 min. The site 5 has a vent that forms a 0.8 m × 0.4 m pool, and a 1 m eruption column for 30 s every 40 min. All times are approximate and are not based on monitoring data covering many eruptions. At a similar elevation on the NW side of the river we observed visually one geyser, a few active vents, and sinter deposits (Fig. 2c). In the upper part of the hydrothermally altered zone, we observed steaming vents without sinter (Fig. 2c).We mapped the NW side of the river by analyzing the UAV images and videos (e.g. Fig. 2a, supplementary material: Video S2).

4.2. Hydrogeochemistry of the geyser area

Thermal waters from geysers and perpetual spouters were at the boiling point (~95.4 °C at an altitude of 1360 m), with pH neutral to slightly alkaline (7 to 8.6), and have electrical conductivities from 1800 to 2100 μS/cm. Mud pools have temperatures between 70 and 90 °C, low pH (2.8 to 3.8) and electrical conductivity of

Fig. 3. (a) Panoramic view of Alpehue canyon looking north toward the Laima volcano (Fig. 1a), (b) UAV view of sinter deposits looking at site 3, (c) sinter deposit laying on breccia at site 4, (d) geyser eruption at site 2, (d) mud pool breaking old sinter at site 5, and (f) hot spring in the river at site 8.

500–800 μS/cm. The thermal springs along the river walls have sub-boiling temperatures (<70 °C). Geochemically, thermal manifestations and meteoric (river) water are distinct; concentrations of major elements are two to three orders of magnitude higher in thermal waters than in the river water (Table 1). The most abundant ions in the thermal water are Cl (385.2 to 430 mg/L), Na (372.0 to 423.5 mg/L), SiO_2 (369.3 to 412.7 mg/L), HCO_3 (99.2 to 179.0 mg/L), and SO_4 (75.8 to 87.5 mg/L). The most abundant trace elements in the thermal waters are B (13.9 to 15.6 mg/L), Li (1.4 to 1.6 mg/L), and As (1.0 to 1.3 mg/L). Note that this As concentration exceeds drinking water standards by two orders of magnitude. Our data are consistent with previous geochemical analyses by Lemus and Honores (2019). The high Cl concentrations, and the relationships between Cl, HCO_3, SO_4 in geysers and perpetual spouters indicate mature geothermal waters (Fig. 4a, Giggenbach, 1988). Compositionally, the mud pool is close to the volcanic water field and the sub-boiling manifestations in the river are within the range of peripheral waters (Lemus and Honores, 2019). The relationship between the conservative elements Li, Cl, B (Fig. 4b, Giggenbach, 1988) and B/Cl ratios (0.02 to 0.04) provides a first-order approximation about the origin of the fluids and water-rock interaction. Those values are similar in all samples indicating geothermal fluids with a common source, which originated from the interaction with a rhyolitic (or a silica-rich) rock (Fig. 4b).

The hydrogen and oxygen isotopic signature of meteoric water (river) at Alpehue, expressed as δD and $\delta^{18}O$ values (Fig. 4c and d), agrees with the local meteoric line (LMWL, Sánchez-Murillo et al., 2018). The sub-boiling feature also agrees with the LMWL. Thermal waters of geysers and perpetual spouters, in contrast, are enriched in D and ^{18}O with respect to local meteoric water. The mud pool has the largest enrichment in both isotopes. Mixing of meteoric water with magmatic fluids can explain a wide range of δD and $\delta^{18}O$ signatures (Giggenbach and Stewart, 1982). However, the local meteoric water (rivers in the area, Sánchez et al., 2013; Munoz, 2011) show a similar δD to geysers and perpetual spouters in Alpehue supporting the notion that water rock-interaction alone can explain the enrichment in ^{18}O. Alternatively, the relatively small enrichment in D of thermal water with respect to meteoric water can be indicative of boiling/evaporation in the subsurface (e.g., D'amore and Panichi, 1985). Regardless of the interpretation,

Table 1
Water geochemistry analyzed for this work (sites 1,3,5,7,9; Fig. 2) and sites reported by Lemus and Honores (2019) represented by notation **. The notation nr correspond to non-reported data.

Sample site	1	1**	3	3**	4**	5	5**	6**	7	7** (mud pool)	8**
Sample ID	ALP01	ALP21ML	ALP03	ALP10ML	ALP22ML	ALP05	ALP20ML	ALP12ML	ALP07	ALP23ML	ALP18ML
Lat (S)	38°59′11.1″	38°59′11.1″	38°59′11.6″	38°59′11.6″	38°59′12.1″	38°59′14.1″	38°59′14.1″	38°59′15.6″	38°59′17.3″	38°59′16.7″	38°59′13.6″
Long (W)	71°35′53.4″	71°35′53.4″	71°35′55.1″	71°35′55.1″	71°35′54.5″	71°35′54.9″	71°35′54.9″	71°35′55.4″	71°35′54.5″	71°35′53.5″	71°35′58.2″
Date	1/10/19	4/24/17	1/10/19	2/25/15	4/24/17	1/10/19	2/25/15	2/25/15	1/10/19	4/24/17	2/25/15
T (°C)	95.4	95.1	95.4	94.5	95	95.4	94.3	93.4	95.4	88.7	<95.4
EC (μS/cm)	1846	1907	2066	1811	1738	1832	1818	1876	2100	499	316
pH	7.20	7.98	8.30	8.56	8.20	7.80	8.28	9.12	8.60	3.38	7.74
Cl (mg/L)	429.98	455.95	416.73	396.00	406.27	395.18	402.00	423.00	385.19	70.74	31.10
F (mg/L)	2.80	3.04	2.63	2.82	3.22	3.73	<0,03	4.12	3.99	0.50	0.53
Br (mg/L)	1.04	nr	1.07	nr	nr	0.98	nr	nr	0.95	nr	nr
SO_4 (mg/L)	77.22	86.05	75.79	82.40	89.25	87.54	91.20	99.20	83.90	88.10	38.50
HCO_3 (mg/L)	179.00	205.59	101.90	219.43	217.98	99.20	176.00	141.10	110.10	nr	84.60
CO_3 (mg/L)	5.50	16.00	12.60	18.69	25.00	5.20	5.10	71.93	11.40	nr	nr
Ca (mg/L)	2.14	2.00	1.88	35.00	3.00	2.73	35.00	40.00	1.43	15.00	10.00
Na (mg/L)	396.00	380.00	423.50	335.00	355.00	390.50	335.00	340.00	372.00	27.30	49.00
K (mg/L)	27.51	23.50	27.51	19.00	19.00	23.21	8.50	18.50	23.15	8.00	5.80
Mg (mg/L)	<0.07	<0.1	<0.07	1.00	<0,1	<0.07	1.00	1.00	<0.07	1.30	2.40
SiO_2 (mg/L)	392.20	284.51	412.70	209.64	263.12	369.30	319.00	209.64	372.90	156.16	111.00
Li (mg/L)	1542. 2	1.95	1401.6	1.40	1.97	1561.5	0.85	1.25	1485.9	0.34	0.05
B (mg/L)	15.60	12.84	15.15	11.01	11.95	14.57	9.88	11.60	13.90	2.54	0.06
As (mg/L)	1.29	0.98	0.98	1.03	0.41	1.17	0.62	1.33	1.03	0.06	0.03
δ^{18}O ‰ (VSMOW)	−7.38	−7.40	−7.57	−7.12	−7.13	−6.45	−7.08	−6.69	−7.38	−4.17	nr
δD ‰ (VSSMOW)	−64.59	−68.16	−67.11	−67.64	−63.71	−61.48	−70.65	−67.88	−62.87	−54.39	nr

the isotope data indicate a dominantly meteoric origin for thermal fluids at Alpehue.

4.3. Sinter deposits and silica phases

Small sinter cones and sinter mounds developed around the geysers and perpetual spouters, and long fan-like aprons are formed downhill on the steep slopes toward the river, up to 40 m from the vents (Fig. 3a, b). The thickness of the sinter varies from 1 m near the vent to a few cm in distal environments. Proximal environments are characterized by columnar (Fig. 5a) and spicular (Fig. 5b) geyserite textures generated by splashing and spraying water from vents at T >75 °C (White, 1967; Walter, 1976). The largest active geyser at site 2 has a splash zone of 3.4 m (Fig. 3d), while the other small geysers and perpetual spouters reach up to 1 m. Near-vent outflow channels and shallow pools present digitated structures with discontinuous and finely laminated sinter that has been associated with intermittent overflow. High slopes and mid apron environments (<75 °C) are characterized by the predominance of micro-terraces (dam <3 cm diameter, Fig. 5d, e). Abundant colorful orange to brown bacterial mats inhabit these areas (Fig. 3b, c, Fig. 5f), and streamer textures are preserved in sinter deposits in discharge channels (Fig. 5e). Distal environments are characterized by sinter stalactites (Fig. 5g) and low temperature nodular and botryoidal geyserite-like textures (Fig. 5h). Geyserite-like textures are formed on the steep river flanks, where low-temperature waters splash on the ground. Low temperature geyserite-like textures are surrounded by green bacterial mats and algae. The SEM images indicate the presence of abundant filamentous bacteria and diatoms inhabiting these environments (Fig. 5i). We observed silicified grass remains in mid and low temperature environments; owing to the abundance of grass in the area, dead plants can fall in channels and pools.

Changes in the vent dynamics are suggested by the overlap of textures from different environments and microscale desiccation cracks. For instance, we observe microscale desiccation cracks within geyserite textures (Fig. 5c), or micro-terraces and desiccation marks secondarily filled by spicules (water splash). We found several small old vents with sinter topographically above the current active vent in site 1, which are currently dominated by mud pools (Fig. 5e). We also observed active sinter vents at site 7 breaking up old sinter terraces.

Analyzing the silica phases from old and active sinter, we found that opal-A is the dominant phase in all samples (Fig. 6, and Fig. S1 supplementary figure). Wide peaks in the XRD spectra indicate values of Full Width at Half Maximum (FWHM) angle between 7.7 and 8.9. The main accessory mineral was plagioclase, which is present in detrital grains from the basaltic to andesitic surrounding rocks. SEM images show the presence of micro-spheres of opal-A in all samples.

4.4. Sinter ages

In one of the old vents at site 1, we obtained a radiocarbon age of 7.37 ± 0.02 ka CalBP and δ^{13}C of −20.5, and in the old deposits of site 7 we obtained two ages of 3.05 ± 0.02 and 3.53 ± 0.02 ka CalBP, and δ^{13}C of −24.2‰ and − 23.8‰, respectively. Values of δ^{13}C between −20‰ and −25‰ are associated with vegetation (e.g., Stuiver and Polach, 1977) and photosynthetic cyanobacteria (e.g., Sakata et al., 1997; Popp et al., 1998; Jahnke et al., 2004), consistent with the material that we dated. Radiocarbon ages from sinter can be compromised by the incorporation of ^{14}C-dead carbon (e.g., Churchill et al., 2020). The signature of such contamination would be more positive δ^{13}C ratios due to enrichment in ^{13}C compared to organic carbon from uncontaminated vegetation and cyanobacteria (Munoz-Saez et al., 2020). The absence of a δ^{13}C evidence of contamination and the similarity of the duplicates suggest that the ages are reliable and representative of sinter formation.

5. Discussion

5.1. Characteristics and origin of the fluids

The geochemical characteristics of thermal waters including mature, chloride-alkaline waters, and silica-rich sinter deposits indicate the presence of a high enthalpy geothermal reservoir at depth (e.g., Giggenbach, 1988; Lynne, 2013). Alpehue combines all these characteristics and the classical geothermometers applied to our 4 samples (Table 2, Fournier and Truesdell, 1973; Fournier, 1977, 1979; Fouillac and Michard, 1981; Giggenbach, 1988) indicate reservoir temperatures averaging between 189.2 ± 5.1 °C (geothermometer Na/K Fournier, 1979) to 254.9 ± 5.8 °C (geothermometer Na/K Giggenbach, 1988). In addition to the classical chemical geothermometers and the ionic relationships, we use a more complex multireaction chemical equilibria

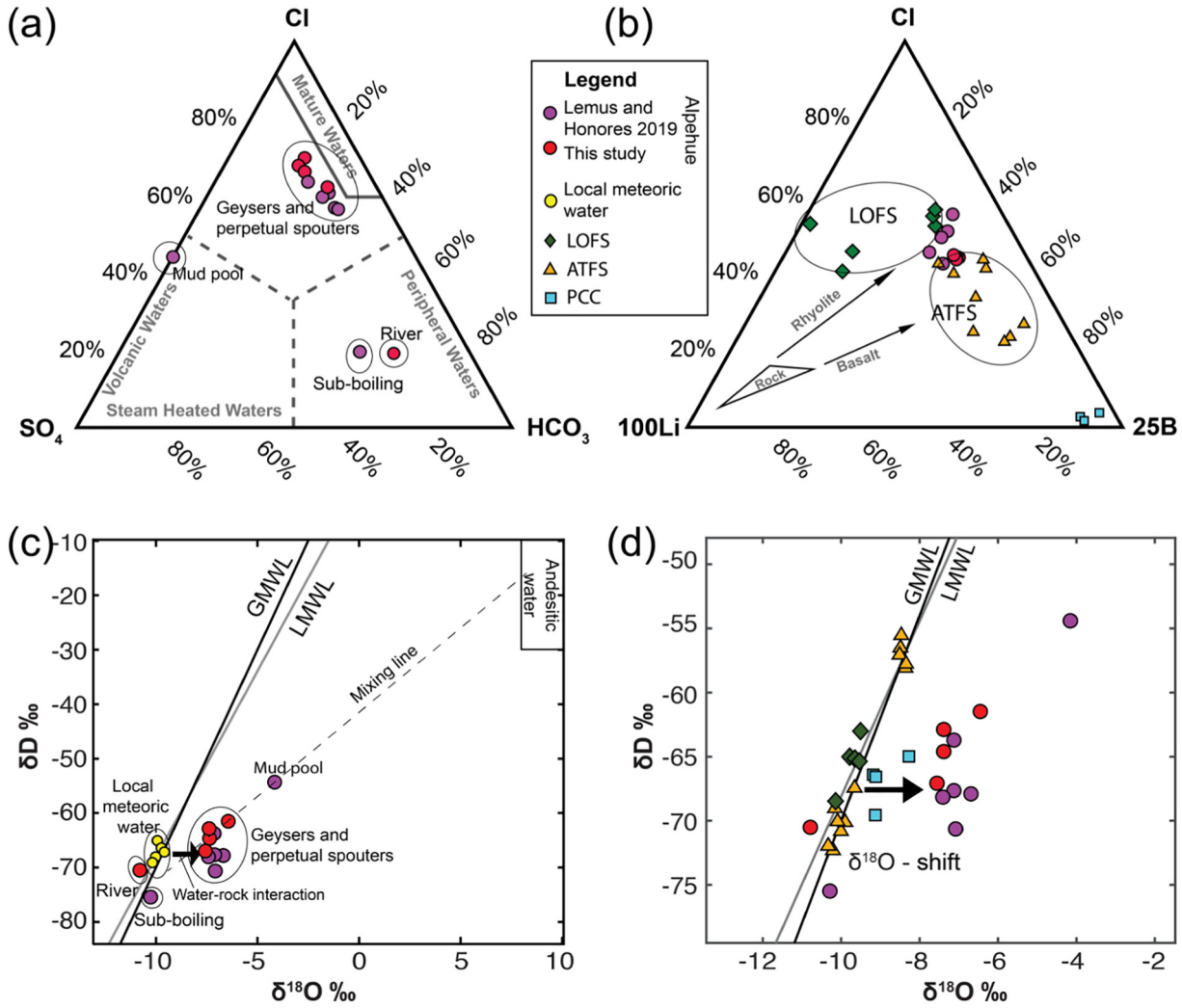

Fig. 4. (a) Ternary diagram for a general classification of geothermal waters in Alpehue for this work and Lemus and Honores (2019). (b) Ternary diagram of conservative elements comparing Alpehue and the thermal waters between the Llaima and Villarica Volcanoes associated with the Liquiñe-Ofqui Fault System (LOFS), the chloride waters associated with the Andean Traverse Fault System (ATFS) (Sánchez et al., 2013; Wrage et al., 2017), and high-silica thermal waters in Puyehue Cordon Caulle (PCC) (Sepúlveda et al., 2004). (c) Stables isotopes comparing Alpehue to the river waters in the area (Munoz, 2011; Sánchez et al., 2013). We added as a reference the global meteoric water line (GMWL) and the local meteoric water line (LMWL, of slope m = 6.48, Sánchez-Murillo et al., 2018). (d) Stables isotopes comparing Alpehue to other thermal waters described in (b).

geothermometry (MEG) implemented in the iGeoT code (Spycher et al., 2013, 2014). For this calculation, we obtain an optimized average temperature of 214.0 ± 5.6 °C, considering all 4 samples and using a mineral assemblage typical of hydrothermal alteration, composed of quartz, sericite, clay minerals, calcite, chlorite, sulfides, epidote and Fe-oxides (e.g., Nicholson, 1992; Berger, 1998). This assemblage is similar to the minerals documented in the closest geothermal wells from the Tolhuaca geothermal system, north of Alpehue (Sanchez-Alfaro et al., 2016). δD and $\delta^{18}O$ signatures of the fluids indicate a dominantly meteoric origin, modulated by water-rock interaction and boiling processes, and/or magmatic addition. The geochemical and isotopic signatures found in Alpehue (Fig. 4c) are relatively uncommon in the SVZ (e.g., Sánchez et al., 2013; Wrage et al., 2017; Lemus and Honores, 2019). Trahuilco, in the Puyehue-Cordon Caulle (PCC) volcanic system at ~40.5°S, is the only previously reported silica-rich system in the SVZ, but it has immature peripheral waters (Sepúlveda et al., 2004) and a smaller $\delta^{18}O$ shift.

Regionally, two main structural systems control the distribution of most of the volcanic centers and geothermal features in the Southern Volcanic Zone (SVZ) (e.g., Lahsen et al., 2010; Sanchez-Alfaro et al., 2016): (a) the Liquiñe-Ofqui Fault System (LOFS), formed by 1200 km long NNE-trending structures, and (b) the Andean Transverse Faults (ATFS), formed by NW-striking structures crossing the arc obliquely and considered pre-Andean crustal weaknesses. Structurally-controlled permeability and underlying basement structures are the two most important first-order controls on fluid flow and reservoir development in the SVZ (Cembrano and Lara, 2009; Sánchez et al., 2013; Tardani et al., 2016; Roquer et al., 2017). The LOFS allows deep circulation of meteoric fluids (~3 km), where fluids heat at depth and fluid-rock interactions generate immature, acidic waters with meteoric isotope signatures, and are characterized by large Cl/B ratios (e.g., Sánchez et al., 2013; Tardani et al., 2016). The ATFS favors long-lived magma reservoirs, which serve as the heat sources for thermal waters (Sánchez et al., 2013; Pérez-Flores et al., 2016). Absorption of magmatic gas, fluid-rock interaction, and dilution lead to a variety of compositions, including mature chloride-alkaline water commonly with higher B/Cl ratios and neutral pH (e.g., Sánchez et al., 2013; Tardani et al., 2016; Wrage et al., 2017). Although the Sollipulli area is regionally bounded by a trace of the LOFS, the composition of the fluids in Alpehue differ greatly from LOFS waters. Locally, Alpehue is at the intersection of the NW and NE-trending structures (López-Escobar et al., 1995; Lemus and Honores, 2019). The Queipue fault coincides with the general NW orientation of the ATFS, and the heat source in Alpehue

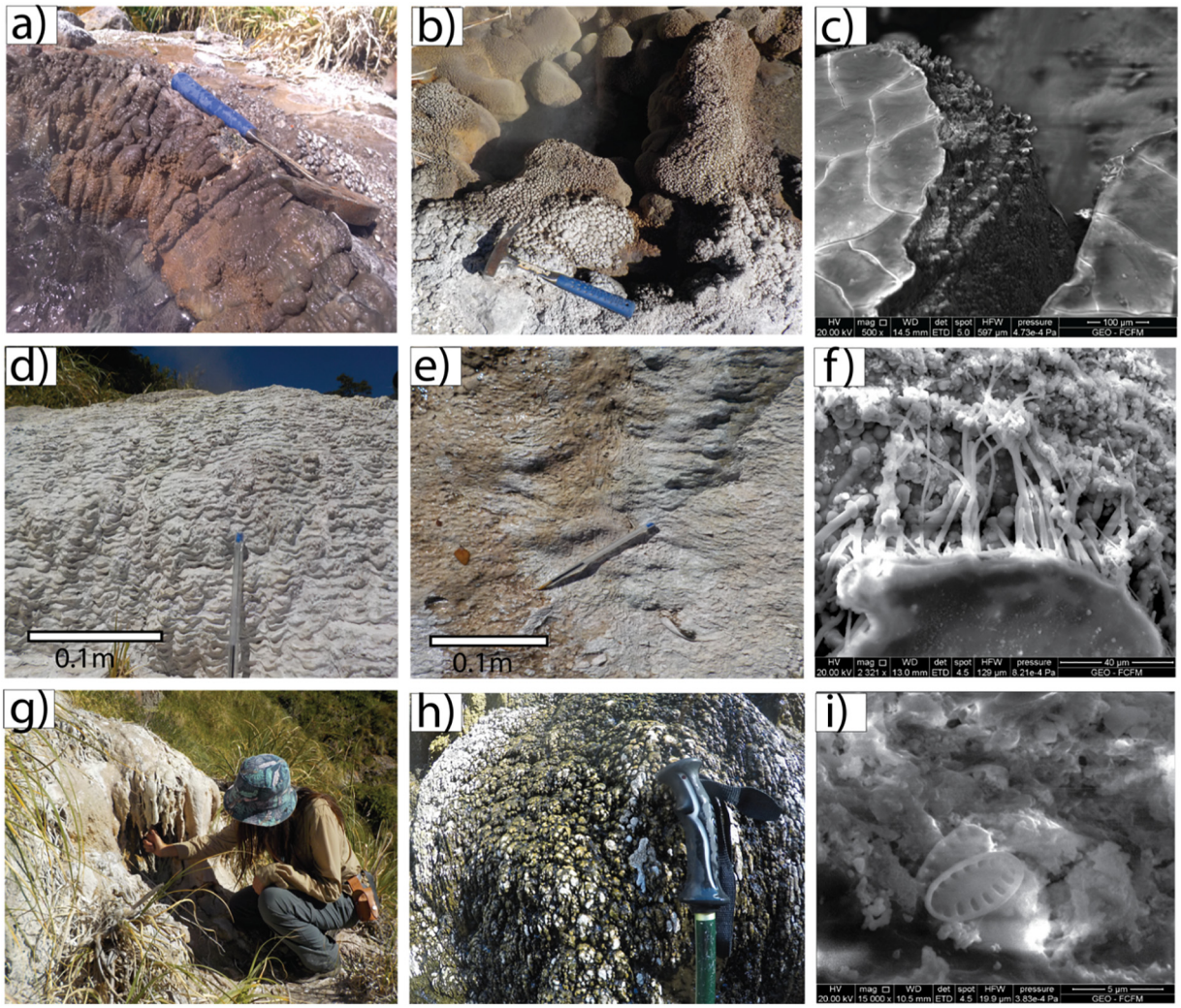

Fig. 5. Proximal deposit or geyserites: (a) columnar texture of a perpetual spouter, (b) spicular texture in geyser splash zone, (c) SEM image of desiccation cracks overlapping micro spicules. Mid environment: (d) micro terraces, (e) streamer fabric, (f) SEM image of microbial filaments. Distal environment: (g) sinter stalactites and plants being covered by sinter, (h) secondary splash texture (geyserite-like), and (i) SEM image of diatoms incorporated into the sinter.

is most likely associated with a magmatic body below the Sollipulli Volcano (Lemus and Honores, 2019). However, compared to Alpehue, the ATFS chloride-alkaline waters commonly are more dilute (SiO_2 values <160 mg/L), have lower temperatures (sub-boiling temperatures between 35 and 80 °C), and δD and $\delta^{18}O$ signatures within the range of local meteoric water (Fig. 4b and d e.g., Sánchez et al., 2013; Wrage et al., 2017). The relationship of conservative elements Li, Cl, B (Fig. 4b) and B/Cl ratios in the thermal waters have shown contrasting signatures in the LOFS and ATFS domain (Sánchez et al., 2013), with higher values of Li and lower B/Cl ratios for the LOFS compared to ATFS systems. However, our data have low Li and intermediate B/Cl without a clear tendency toward any structural system (Fig. 4b).

In this study, we were unable to measure the discharge of thermal waters and hence estimate the heat discharged by this geothermal system, as assessed by Munoz-Saez et al. (2020) for El Tatio. Considering that all thermal features drain to the river, Alpehue may be an ideal location to estimate (in future studies) the heat and mass budgets by using chlorine inventory method (Ingebritsen et al., 1989, 2001).

5.2. Availability of silica and sinter formation

The high SiO_2 content of water discharged by geysers and perpetual spouters in Alpehue (300 to 400 mg/L) is similar to values reported in large geyser fields such as Yellowstone National Park (e.g., Hurwitz and Manga, 2017), and Geyser Flat in New Zealand (e.g., Giggenbach and Glover, 1992), and are even slightly higher than those reported for El Tatio (250 to 320 mg/L; Nicolau et al., 2014; Munoz-Saez et al., 2018). All the above-mentioned geyser fields are characterized by the occurrence of large silica sinter deposits. The ~7.4 ka Cal BP age reported here for Alpehue is similar to older ages in Holocene geyser fields such as Yellowstone ~8.5 ka (Lowenstern et al., 2016) and Steamboat, Nevada ~11.4 ka in the USA (Lynne et al., 2008). In contrast, the El Tatio geyser system in northern Chile is older, with ages up ~27 ka (Slagter et al., 2019; Munoz-Saez et al., 2020). However, it is important to note that the limited number of radiocarbon ages presented here hampers our ability to probe the full sinter history. The lack of silica maturation (predominance of opal A) in Alpehue is also consistent with maturation ages <10 ka (Herdianita et al., 2000), in agreement with our radiocarbon ages.

The main sources of silica in geyser fields around the world are SiO_2-rich rhyolite flows or ignimbrites (e.g., Hurwitz and Manga, 2017). In the CVZ of northern Chile, regional silicic volcanism generated large ignimbrites sheets from the Miocene to the Pleistocene, which provide abundant silica to generate the large sinter deposits reported by Tassi et al. (2010). Other factors, such as the long-term continuous hydrothermal activity and high evaporation in the extremely arid Atacama Desert climate, favor the development of large hydrothermal deposits. For instance, El Tatio has developed ~10 km^2 of silica deposits (e.g., Munoz-Saez et al., 2016, 2018; Slagter et al., 2019) since the late

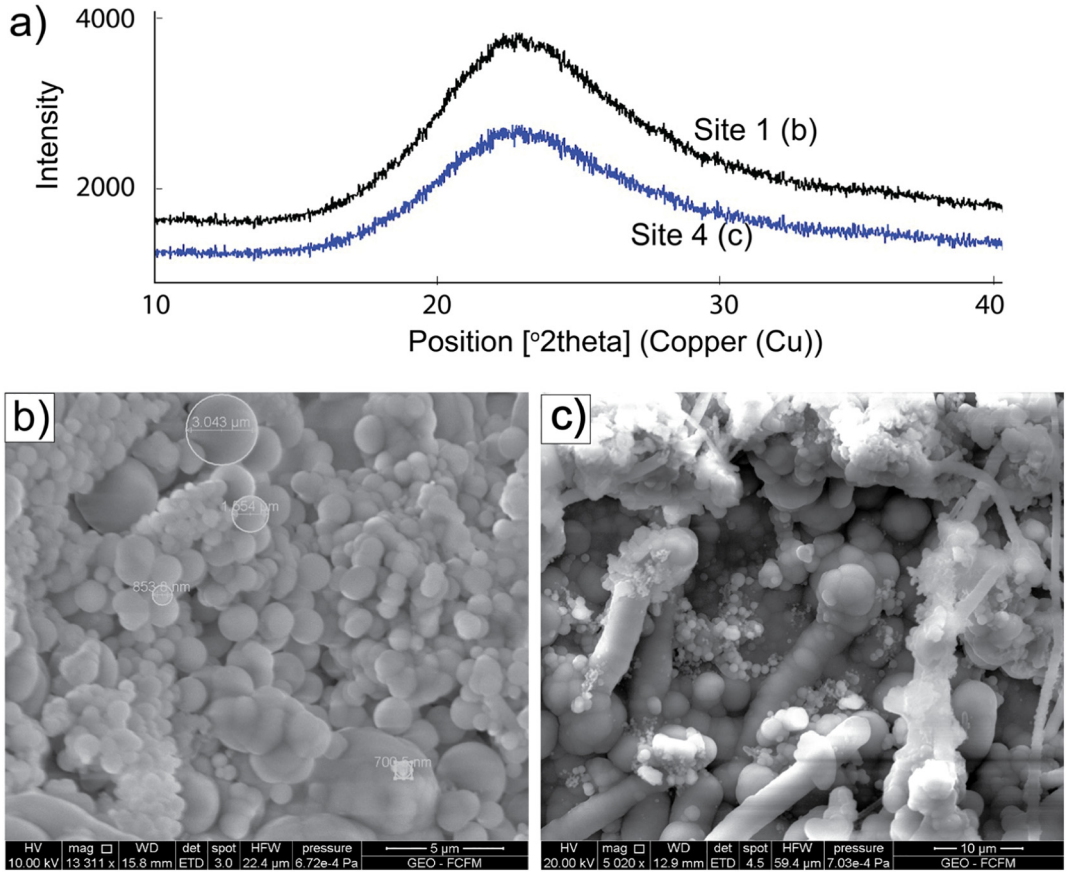

Fig. 6. Opal A is the dominant silica phase, examples from sites 1 and 4. (a) XRD diffractogram, (b) SEM microspheres showing opal A at site 1, figure includes measurements of size of the spheres, and (c) SEM showing opal A at site 4 along with bacterial filaments incorporated into the sinter. More details of the XRD patterns are included in Fig. S1.

Pleistocene (Munoz-Saez et al., 2020). In contrast, Quaternary volcanism in the SVZ is predominately basaltic to andesitic, and silica-rich flows and ignimbrites are more unusual (Lara et al., 2006). This difference may explain the rarity of finding sinter deposits in the SVZ. Only small active sinter vents have been reported in the SVZ at Pueyehue Cordon-Caulle area (Sepúlveda et al., 2004), here at the Sollipulli Volcano, and old sinter mounds were described at Tolhuaca (Melosh et al., 2012). There is evidence of rhyolitic eruptions occurring the last 100 ka in the Puyehue Cordon-Caulle system (e.g., Lara et al., 2006; Naranjo et al., 2017). The Sollipulli Volcano follows the general trend of producing predominately andesites and basalts (e.g., Naranjo et al., 1993). However, a few higher-silica dacites and trachydacites exist to the northwest, in the Circum-caldera and Alpehue units (Fig. 1 Lachowycz et al., 2015). The Alpehue volcanic unit is closest to the hydrothermal field, but it is younger (~2.9 ka, Naranjo et al., 1993; Lachowycz et al., 2015) than the hydrothermal field (~7.4 ka Cal BP). Also, it is likely that some silica may be sourced from Miocene intrusive bodies of granodioritic composition that are recognized in the area (Naranjo et al., 1993; Sánchez et al., 2013).

5.3. Effects of the local geology and landscape

Most of large geyser fields around the world developed in relatively flat basins with glacial deposits underlying silica sinters (e.g. Yellowstone, El Tatio, Geyser Flat; Hurwitz and Manga, 2017). Geysers, perpetual spouters, and sinter mounds in Alpehue occur in steep terrain, and are restricted to the area covered by a brecciated deposit of unknown origin. This brecciated deposit covers the bottom of a glacial valley. However, glacial deposits, mostly till and hyaloclastites, have been described only on the east side of the Sollipulli Volcano (e.g., Lachowycz et al., 2015). The fact that the breccia controls the distribution of surface features at Alpehue strongly suggests that it plays role in the geysering processes. Shallow reservoirs or cavities related to geysering processes have been assumed to occur in the first few meters to tens of meters below the surface (e.g., Weir et al., 1992; Belousov et al., 2013; Wu et al., 2017, 2019; Ardid et al., 2019). Precipitation of silica in a porous and/or fractured lithology such as breccia over a long period (i.e., 7.4 ka Cal BP) may help line the pathways and cavities needed to transport, accumulate and release fluid episodically.

Table 2
Geothermometry based on SiO_2 adiabatic and conductive (Fournier, 1977), Na/K (Fournier, 1979), Na/K (Giggenbach, 1988), Na/Li (Fouillac and Michard, 1981), Na/Li/Ca (Fournier and Truesdell, 1973) and multimineral iGeoT (Spycher et al., 2014).

Site	T_SiO2 adiabatic	T_SiO_2 conductive	T_Na/K Fournier	T_Na/K Giggenbach	T_Na/Li	T_Na/Li/Ca	iGeoT	iGeoT +/−
1	209.0	231.0	195.6	262	197.4	203.0	215.3	27.7
3	212.4	235.4	190.4	256.3	184.7	202.9	221.3	27.7
5	205.1	226.0	183.7	248.6	199.5	189.0	208.7	26.6
7	205.7	226.8	187.1	252.6	199.5	203.2	210.7	26.6
Average	208.1	229.8	189.2	254.9	195.3	199.6	214.0	27.2
Std	3.4	4.3	5.1	5.8	7.1	7.0	5.6	0.6

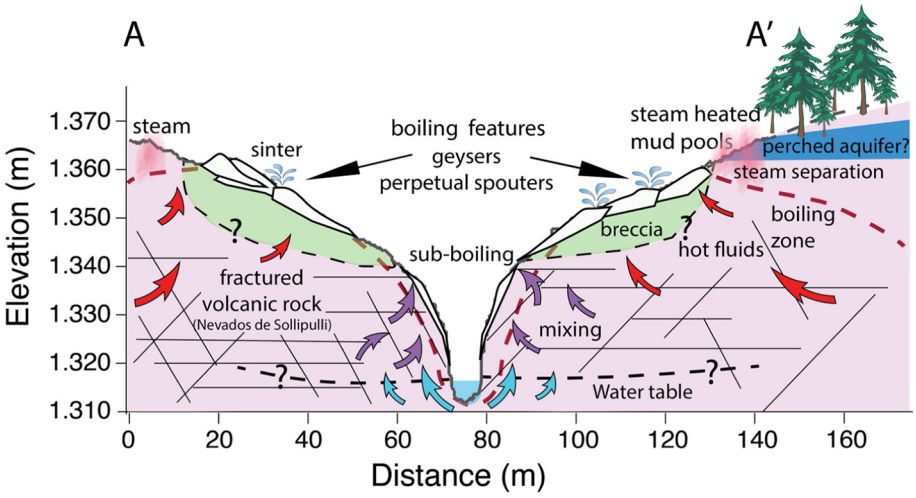

Fig. 7. Topographic distribution of hydrothermal features and proposed conceptual model for fluid circulation at Alpehue. The lithological units are the same as those described in Fig. 2c.

We infer that geysers and perpetual spouters develop when boiling water is discharged at the surface (Fig. 7). The ability of boiling fluids to reach the surface is facilitated by the incision from the river, suggesting a relationship between landscape evolution and hydrothermal activity. River erosion over time could have incised into a potential reservoir clay cap that previously kept in the reservoir confined. This opening can result in depressurization of water the reservoir and boiling. Numerical simulations indicate that fast erosion increases the discharge rate of thermal fluids (Kiryukhin et al., 2012).

The water geochemistry and its δD - $\delta^{18}O$ composition indicate that peripheral sub-boiling features on the riverbanks (below 1350 m elevation) are diluted and cooled by mixing with meteoric water from the river that infiltrates the highly fractured volcanic rock. Lemus and Honores (2019) suggested the contact between volcanic units from the Mid and Late Pleistocene in the Nevados de Sollipulli group dominate the permeability in this area. Formation of thin layers of sinter may be due to the dilution of silica in the water.

Acid-sulphate water in mud pools at higher elevations on the southeast side of the river above the boiling zone (elevation >1360 m) suggest interaction of ground water (a perched aquifer?) with H_2S and CO_2 separated from the boiling hydrothermal fluid. Oxidation of H_2S in steam-heated features generates acidic waters that alter the surrounding rock, forming clays and native sulfur deposits (e.g. Nicholson, 2012). The diluted water geochemistry in the mud pool reported by Lemus and Honores (2019), and low electrical conductivity measured in water samples of these areas, indicate significant interaction (mixing?) with meteoric fluids. On the northwest side of the river, we observed steam vents in the drone images (Fig. 2c, supplementary material: Video S2), suggesting that there is no shallow, cold aquifer on that side. Due to the steep topography of the Alpehue canyon (Fig. 2), we observe boiling and steam-heated features close to each other. Lowering the elevation of the steam-water interface can expand the zone occupied by acid sulphate waters (e.g., Allis, 1981; Handley and Campbell, 2011; Watts-Henwood et al., 2017). Seasonal changes in the water table can promote the development of mud pools in the sinter area, suggested by field observations of sinter textures from different environments overlapping in several vents and dry mud pools at the same elevation as geysers. Whether this migration can occur on annual time scales, or requires extended droughts or wet periods, cannot be determined without more detailed stratigraphic data and radiocarbon ages.

The steep topography of the Alpehue canyon also has an effect on the sinter deposits, allowing the development of small mounds with long and steep aprons in the direction of the river (higher slope, Fig. 2). Micro-terraces with dams <3 cm in diameter are the most common sinter texture in all environments. Observations in travertine established an empirical relationship where the size of the terrace dam is inversely proportional to the tangent of slope angle in the landscape (e.g., Pentecost, 2005; Viles and Pentecost, 2007). This relationship indicates that the steeper the slope, the smaller the size of the terrace dam. Consistent with this relationship, on Alpehue slopes >40° at Alpehue we observe a predominance of micro-terraces, <1 cm in diameter, on mid/distal aprons. In contrast, the El Tatio geyser field, for example, is a nearly flat basin and the sinter mounds reach up to 2 m, the aprons develop meter size terraces, and platforms of sinter can extend for hundreds of meters. Additionally, the vertical waterfall on the riverbank generates botryoidal, geyserite-like sinter textures associated with secondary splash. Taken together, these observations show that sinter deposits preserve a record of topography, suggesting an unforeseen utility as a proxy for landscape evolution.

6. Conclusions

The Alpehue geothermal field in the SVZ presents a large variety of surface manifestations including geysers, sinters, perpetual spouters, sub-boiling hot springs, and mud pools, in a relatively small area (at least 0.2 km^2). The distribution of these active manifestations is most likely dictated by topographic gradient, lithology, and the position of the water table.

The geochemical and isotopic composition of geysers and perpetual spouters indicate that the chloride-alkaline silica-rich fluids of Alpehue have a dominantly meteoric origin. ^{18}O enrichment indicates the influence of fluid-rock interaction processes, boiling, and/or inputs from a geothermal reservoir with an estimated equilibrium temperature >200 °C at depth. Those fluids generated extensive silica sinter deposits, with radiocarbon ages indicating a longevity of at least ~7.4 ka. Sinter deposits are characterized by textures of micro-terraces that develop on high slopes.

The hydrogeochemical features in Alpehue and its sinter deposits are similar to those in large geyser fields around the world but are very unusual compared to most active geothermal systems in the SVZ. We propose that the steep topography and lithology (hydrothermally-altered breccia) at Alpehue control the movement of the fluids and development of geysers. Furthermore, it is likely that the incision of the river may enable silica-rich boiling water to reach the surface, while continuous fluid circulation and silica precipitation in a porous brecciated rock creates the pathways and cavities needed for geysering. The combination of characteristics found here – steep topography, silica-rich geothermal waters, and high rock permeability – enable the occurrence of geysers outside of the large basins where most of Earth's

geysers appear. Since these conditions exist in regions that are difficult to access, it may be that other small fields similar to Alpehue have yet to be identified and characterized. The conditions that enable these small geothermal manifestations at the surface provide a window to identify and explore subsurface hydrothermal systems.

Supplementary data to this article can be found online at https://doi.org/10.1016/j.jvolgeores.2020.107065.

CRediT authorship contribution statement

Carolina Munoz-Saez: Conceptualization, Methodology, Validation, Formal analysis, Investigation, Writing - original draft, Supervision, Project administration. **Carolina Perez-Nuñez:** Formal analysis, Investigation, Writing - review & editing. **Sebastian Martini:** Conceptualization, Methodology, Supervision, Writing - review & editing. **Alonso Vargas-Barrera:** Formal analysis, Software, Writing - review & editing. **Martin Reich:** Resources, Writing - review & editing. **Diego Morata:** Resources, Funding acquisition. **Michael Manga:** Resources, Funding acquisition, Writing - review & editing.

Declaration of competing interest

The authors declare that they have no known competing financial interests or personal relationships that could have appeared to influence the work reported in this paper.

Acknowledgments

The corresponding author was supported by ANID-FONDECYT Postdoctoral Grant (3170007), and the American Fellowship from the American Association of University Women (AAUW). Additional support for coauthors and field work was provided by ANID-FONDAP project 15090013 “Centro de Excelencia en Geotermia de Los Andes, CEGA and ANID through Millennium Science Initiative Program (NCN13_065) “Millennium Nucleus for Metal Tracing Along Subduction. The US National Science Foundation (EAR1724986) provided isotope and radiocarbon analysis costs. The ICP-MS analytical work was supported by ANID-FONDEQUIP instrumentation grant EQM120098. This study is part of the Fondecyt Regular Grant 1201219 “The optimal geologic conditions that form high enthalpy, metal- rich volcanic-hydrothermal systems in the Andes: Thermodynamic and mechanical numerical approach. Puyehue-Cordon Caulle and Sollipulli Volcanoes”. We thank John Southon from the Keck-Carbon Cycle AMS for the radiocarbon measurements; Veronica Rodriguez for helping with lab procedures and Christian Nievas for helping with the SEM; Rodrigo Carilao from the agro-camping Lleuque to guide us to Alpehue; and the two anonymous reviewers from JVGR for their constructive comments.

References

Allis, R.G., 1981. Changes in heat flow associated with exploitation of Wairakei geothermal field, New Zealand. N. Z. J. Geol. Geophys. 24 (1), 1–19.

Ardid, A., Vera, E., Kelly, C., Manga, M., Munoz-Saez, C., Maksymowicz, A., Ortega-Culaciati, F., 2019. Geometry of geyser plumbing inferred from ground deformation. J. Geophys. Res. Solid Earth 124 (1), 1072–1083.

Belousov, A., Belousova, M., Nechayev, A., 2013. Video observations inside conduits of erupting geysers in Kamchatka, Russia, and their geological framework: implications for the geyser mechanism. Geology 41 (4), 387–390.

Berger, B.R., 1998. Hydrothermal alteration. Geochemistry. Encyclopedia of Earth Science. Springer, Dordrecht.

Campbell, K.A., Sannazzaro, K., Rodgers, K.A., Herdianita, N.R., Browne, P.R.L., 2001. Sedimentary facies and mineralogy of the late Pleistocene Umukuri silica sinter, Taupo Volcanic Zone, New Zealand. J. Sediment. Res. 71 (5), 727–746.

Campbell, K.A., Guido, D.M., Gautret, P., Foucher, F., Ramboz, C., Westall, F., 2015. Geyserite in hot-spring siliceous sinter: window on Earth's hottest terrestrial (paleo) environment and its extreme life. Earth Sci. Rev. 148, 44–64.

Campbell, K.A., Guido, D.M., Vikre, P.G., John, D.A., Rhys, D., Hamilton, A.R., 2019. The Miocene Atastra Creek sinter (Bodie Hills volcanic field, California and Nevada): 4D evolution of a geomorphically intact siliceous hot–spring deposit. J. Volcanol. Geotherm. Res. 370, 65–81. https://doi.org/10.1016/j.jvolgeores.2018.12.006.

Cembrano, J., Lara, L., 2009. The link between volcanism and tectonics in the southern volcanic zone of the Chilean Andes: a review. Tectonophysics 471 (1–2), 96–113.

Churchill, D.M., Manga, M., Hurwitz, S., Peek, S., Licciardi, J.M., Paces, J.B., 2020. Dating Silica Sinter (Geyserite): A Cautionary Tale. https://doi.org/10.1016/j.jvolgeores.2020.106991.

Coleman, M.L., Shepherd, T.J., Durham, J.J., Rouse, J.E., Moore, G.R., 1982. Reduction of water with zinc for hydrogen isotope analysis. Anal. Chem. 54 (6), 993–995.

D'amore, F., Panichi, C., 1985. Geochemistry in geothermal exploration. Int. J. Energy Res. 9 (3), 277–298.

Epstein, S., Mayeda, T., 1953. Variation of O18 content of waters from natural sources. Geochim. Cosmochim. Acta 4 (5), 213–224.

Farmer, J., 1998. Thermophiles, early biosphere evolution, and the origin of life on Earth: implications for the exobiological exploration of Mars. J. Geophys. Res. Planets 103 (E12), 28457–28461.

Farmer, J.D., 2000. Hydrothermal systems: doorways to early biosphere evolution. GSA Today 10 (7), 1–9.

Farmer, J.D., Des Marais, D.J., 1999. Exploring for a record of ancient Martian life. J. Geophys. Res. Planets 104 (E11), 26977–26995.

Fouillac, R., Michard, S., 1981. Sodium/Lithium ratio in water applied to geothermometry of geothermal reservoirs. Geothermics 10, 55–70. https://doi.org/10.1016/0375-6505(81)90025-0.

Fournier, R.O., 1977. Chemical geothermometers and mixing models for geothermal systems. Geothermics 5 (1–4), 41–50.

Fournier, R.O., 1979. Geochemical and hydrologic considerations and the use of enthalpy-chloride diagrams in the prediction of underground conditions in hot-spring systems. J. Volcanol. Geotherm. Res. 5 (1–2), 1–16.

Fournier, R.O., Rowe, J.J., 1966. Estimation of underground temperatures from the silica content of water from hot springs and wet-steam wells. Am. J. Sci. 264 (9), 685–697.

Fournier, R.O., Truesdell, A.H., 1973. An empirical Na K Ca geothermometer for natural waters. Geochim. Cosmochim. Acta 37 (5), 1255–1275.

Giggenbach, W.F., 1988. Geothermal solute equilibria. Derivation of Na-K-Mg-Ca geoindicators. Geochim. Cosmochim. Acta 52 (12), 2749–2765.

Giggenbach, W.F., 1989. Collection and analysis of geothermal and volcanic water and gas discharges. NZ DSIR Chem. Rep. 2401, 1–82.

Giggenbach, W.F., Stewart, M.K, 1982. Processes controlling the isotopic composition of steam and water discharges from steam vents and steam-heated pools in geothermal areas. Geothermics 11 (2), 71–80.

Giggenbach, W.F., Glover, R.B., 1992. Tectonic regime and major processes governing the chemistry of water and gas discharges from the Rotorua geothermal field, New Zealand. Geothermics 21 (1–2), 121–140.

Gilbert, J.S., Stasiuk, M.V., Lane, S.J., Adam, C.R., Murphy, M.D., Sparks, R.S.J., Naranjo, J.A., 1996. Non-explosive, constructional evolution of the ice-filled caldera at Volcán Sollipulli, Chile. Bull. Volcanol. 58 (1), 67–83.

Guido, D.M., Campbell, K.A., Foucher, F., Westall, F., 2019. Life is everywhere in sinters: examples from Jurassic hot-spring environments of Argentine Patagonia. Geol. Mag. 156 (9), 1631–1638.

Hamilton, A.R., Campbell, K.A., Rowland, J.V., Barker, S., Guido, D.M., 2018. Characteristics and variations of sinters in the Coromandel Volcanic Zone: application to epithermal exploration. N. Z. J. Geol. Geophys. https://doi.org/10.1080/00288306.2018.1519514.

Hamilton, A.R., Campbell, K.A., Guido, D.M., 2019a. Atlas of Siliceous Hot Spring Deposits (Sinter) and Other Silicified Surface Manifestations in Epithermal Environments. GNS Science, Te Pū Ao.

Hamilton, A.R., Campbell, K.A., Rowland, J.V., Barker, S., Guido, D.M., 2019b. Fossilised geothermal surface features of the Whitianga Volcanic Centre (Miocene), Coromandel Volcanic Zone, New Zealand: Controls and characteristics. J. Volcanol. Geotherm. Res. 381, 209–226.

Handley, K.M., Campbell, K.A., 2011. Character, analysis, and preservation of biogenicity in terrestrial siliceous stromatolites from geothermal settings. Stromatolites: Interaction of Microbes with Sediments. Springer, Dordrecht, pp. 359–381.

Herdianita, N.R., Browne, P.R.L., Rodgers, K.A., Campbell, K.A., 2000. Mineralogical and textural changes accompanying ageing of silica sinter. Mineral. Deposita 35 (1), 48–62.

Hobbs, L.K., 2014. The Role of Cold Superglacial Volcanic Deposits in Influencing Glacial Ablation. PhD thesis. Lancaster University, UK.

Hogg, A.G., Hua, Q., Blackwell, P.G., Niu, M., Buck, C.E., Guilderson, T.P., Heaton, T.J., Palmer, J.G., Reimer, P.J., Reimer, R.W., Turney, C.S., 2013. SHCal13 Southern Hemisphere calibration, 0–50,000 years cal BP. Radiocarbon 55 (4), 1889–1903.

Howald, T., Person, M., Campbell, A., Lueth, V., Hofstra, A., Sweetkind, D., Gable, C.W., Banerjee, A., Luijendijk, E., Crossey, L., Karlstrom, K., 2014. Evidence for long timescale (> 103 years) changes in hydrothermal activity induced by seismic events. Geofluids 15 (1–2), 252–268.

Hurwitz, S., Manga, M., 2017. The fascinating and complex dynamics of geyser eruptions. Annu. Rev. Earth Planet. Sci. 45, 31–59.

Hurwitz, S., Kumar, A., Taylor, R., Heasler, H., 2008. Climate-induced variations of geyser periodicity in Yellowstone National Park, USA. Geology 36 (6), 451–454.

Husen, S., Taylor, R., Smith, R.B., Healser, H., 2004. Changes in geyser eruption behavior and remotely triggered seismicity in Yellowstone National Park produced by the 2002 M 7.9 Denali fault earthquake, Alaska. Geology 32 (6), 537–540.

Ingebritsen, S.E., Rojstaczer, S.A., 1993. Controls on geyser periodicity. Science 262 (5135), 889–892.

Ingebritsen, S.E., Rojstaczer, S.A., 1996. Geyser periodicity and the response of geysers to deformation. J. Geophys. Res. Solid Earth 101 (B10), 21891–21905.

Ingebritsen, S.E., Sherrod, D.R., Mariner, R.H., 1989. Heat flow and hydrothermal circulation in Cascade range, north-central Oregon. Science 243, 1458–1462.

Ingebritsen, S.E., Galloway, D.L., Colvard, E.M., Sorey, M.L., Mariner, R.H., 2001. Time-variation of hydrothermal discharge at selected sites in the western United States: implications for monitoring. J. Volcanol. Geotherm. Res. 111 (1), 1–23.

Jahnke, L.L., Embaye, T., Hope, J., Turk, K.A., Van Zuilen, M., Des Marais, D.J., Farmer, J.D., Summons, R.E., 2004. Lipid biomarker and carbon isotopic signatures for stromatolite-forming, microbial mat communities and Phormidium cultures from Yellowstone National Park. Geobiology 2 (1), 31–47.
Kedar, S., Kanamori, H., Sturtevant, B., 1998. Bubble collapse as the source of tremor at Old Faithful Geyser. J. Geophys. Res. Solid Earth 103 (B10), 24283–24299.
Kieffer, S.W., 1989. Geologic nozzles. Rev. Geophys. 27 (1), 3–38.
Kiryukhin, A.V., Rychkova, T.V., Dubrovskaya, I.K., 2012. Formation of the hydrothermal system in Geysers Valley (Kronotsky Nature Reserve, Kamchatka) and triggers of the Giant Landslide. Appl. Geochem. 27 (9), 1753–1766.
Konhauser, K.O., Jones, B., Reysenbach, A.L., Renaut, R.W., 2003. Hot spring sinters: keys to understanding Earth's earliest life forms. Can. J. Earth Sci. 40, 1713–1724.
Lachowycz, S.M., Pyle, D.M., Gilbert, J.S., Mather, T.A., Mee, K., Naranjo, J.A., Hobbs, L.K., 2015. Glaciovolcanism at Volcán Sollipulli, southern Chile: lithofacies analysis and interpretation. J. Volcanol. Geotherm. Res. 303, 59–78.
Lahsen, A., Muñoz, N., Parada, M.A., 2010, April. Geothermal development in Chile. In Proceedings world geothermal congress, Bali. Indonesia 25–29.
Lara, L.E., Lavenu, A., Cembrano, J., Rodríguez, C., 2006. Structural controls of volcanism in transversal chains: resheared faults and neotectonics in the Cordón Caulle–Puyehue area (40.5 S), Southern Andes. J. Volcanol. Geotherm. Res. 158 (1–2), 70–86.
Lemus, M., Honores, C., 2019. Favorabilidad geotérmica de la cordillera Principal de la región de La Araucanía. Servicio Nacional de Geología y Minería, Informe Registrado IR-19-75 178 p. (2 mapas escala 250.000. Santiago).
López-Escobar, L., Cembrano, J., Moreno, H., 1995. Geochemistry and tectonics of the Chilean Southern Andes basaltic Quaternary volcanism (37-46 S). Andean Geol. 22 (2), 219–234.
Lowenstern, J.B., Hurwitz, S., McGeehin, J.P., 2016. Radiocarbon dating of silica sinter deposits in shallow drill cores from the Upper Geyser Basin, Yellowstone National Park. J. Volcanol. Geotherm. Res. 310, 132–136.
Lynne, B.Y., 2012. Mapping vent to distal-apron hot spring paleo-flow pathways using siliceous sinter architecture. Geothermics 43, 3–24.
Lynne, B.Y., 2013. Siliceous sinter: an early exploration tool and direct link to a geothermal reservoir. Thirty-Eight Work. Geotherm. Reserv. Eng 1–6.
Lynne, B.Y., Campbell, K.A., Moore, J., Browne, P.R.L., 2008. Origin and evolution of the Steamboat Springs siliceous sinter deposit, Nevada, USA. Sediment. Geol. 210 (3–4), 111–131.
Melosh, G., Moore, J., Stacey, R., 2012. Natural reservoir evolution in the Tolhuaca geothermal field, southern Chile. 37th Workshop on Geothermal Reservoir Engineering Stanford University, Stanford, California, January 31–February 1, 2012. SGP-TR-194.
Munoz, M., 2011. Sistema Geotermal Asociado al Volcán Sierra Nevada: Estudio Geoquímico de Aguas y Gases Termales. Universidad de Chile - Facultad de Ciencias Físicas y Matemáticas, Santiago, Chile http://repositorio.uchile.cl/handle/2250/104245.
Munoz-Saez, C., Manga, M., Hurwitz, S., Rudolph, M.L., Namiki, A., Wang, C.Y., 2015a. Dynamics within geyser conduits, and sensitivity to environmental perturbations: insights from a periodic geyser in the El Tatio geyser field, Atacama Desert, Chile. J. Volcanol. Geotherm. Res. 292, 41–55.
Munoz-Saez, C., Namiki, A., Manga, M., 2015b. Geyser eruption intervals and interactions: examples from El Tatio, Atacama, Chile. J. Geophys. Res. Solid Earth 120 (11), 7490–7507.
Munoz-Saez, C., Saltiel, S., Manga, M., Nguyen, C., Gonnermann, H., 2016. Physical and hydraulic properties of modern sinter deposits: El Tatio, Atacama. J. Volcanol. Geotherm. Res. 325, 156–168.
Munoz-Saez, C., Manga, M., Hurwitz, S., 2018. Hydrothermal discharge from the El Tatio basin, Atacama, Chile. J. Volcanol. Geotherm. Res. 361, 25–35.
Munoz-Saez, C., Manga, M., Hurwitz, S., Slagter, S., Churchill, D.M., Reich, M., Damby, D., Morata, D., 2020. Radiocarbon dating of silica sinter and postglacial hydrothermal activity in the El Tatio geyser field. Geophys. Res. Lett. 47 (11) e2020GL087908.
Murphy, M.D., 1996. Magmatic Evolution at Volcan Sollipulli, Southern Andes of Chile. Doctoral dissertation. University of Bristol.
Naranjo, J.A., Moreno, H., Emparan, C., Murphy, M., 1993. Volcanismo explosivo reciente en la caldera del volcán Sollipulli, Andes del Sur (39 S). Andean Geol. 20 (2), 167–191.
Naranjo, J.A., Singer, B.S., Jicha, B.R., Moreno, H., Lara, L.E., 2017. Holocene tephra succession of Puyehue-Cordón Caulle and Antillanca/Casablanca volcanic complexes, southern Andes (40–41 S). J. Volcanol. Geotherm. Res. 332, 109–128.
Nicholson, K., 1992. Environmental impact of geothermal resources: examples from New Zealand. Renewable Energy: Technology and the Environment. V. 5: Related Topics.
Nicholson, K., 2012. Geothermal Fluids: Chemistry and Exploration Techniques. Springer Science & Business Media.
Nicolau, C., Reich, M., Lynne, B., 2014. Physico-chemical and environmental controls on siliceous sinter formation at the high-altitude El Tatio geothermal field, Chile. J. Volcanol. Geotherm. Res. 282, 60–76.
Pentecost, Allan, 2005. Travertine. Springer Science & Business Media.
Pérez-Flores, P., Cembrano, J., Sánchez-Alfaro, P., Veloso, E., Arancibia, G., Roquer, T., 2016. Tectonics, magmatism and paleo-fluid distribution in a strike-slip setting: Insights from the northern termination of the Liquiñe–Ofqui fault System, Chile. Tectonophysics 680, 192–210.
Popp, B.N., Laws, E.A., Bidigare, R.R., Dore, J.E., Hanson, K.L., Wakeham, S.G., 1998. Effect of phytoplankton cell geometry on carbon isotopic fractionation. Geochim. Cosmochim. Acta 62 (1), 69–77.
Rojstaczer, S., Galloway, D.L., Ingebritsen, S.E., Rubin, D.M., 2003. Variability in geyser eruptive timing and its causes: Yellowstone National Park. Geophys. Res. Lett. 30 (18).
Roquer, T., Arancibia, G., Rowland, J., Iturrieta, P., Morata, D., Cembrano, J., 2017. Fault-controlled development of shallow hydrothermal systems: structural and mineralogical insights from the Southern Andes. Geothermics 66, 156–173.
Sakata, S., Hayes, J.M., McTaggart, A.R., Evans, R.A., Leckrone, K.J., Togasaki, R.K., 1997. Carbon isotopic fractionation associated with lipid biosynthesis by a cyanobacterium: relevance for interpretation of biomarker records. Geochim. Cosmochim. Acta 61 (24), 5379–5389.
Sánchez, P., Pérez-Flores, P., Arancibia, G., Cembrano, J., Reich, M., 2013. Crustal deformation effects on the chemical evolution of geothermal systems: the intra-arc Liquiñe–Ofqui fault system, Southern Andes. Int. Geol. Rev. 55 (11), 1384–1400.
Sanchez-Alfaro, P., Reich, M., Arancibia, G., Pérez-Flores, P., Cembrano, J., Driesner, T., Lizama, M., Rowland, J., Morata, D., Heinrich, C.A., Tardani, D., 2016. Physical, chemical and mineralogical evolution of the Tolhuaca geothermal system, southern Andes, Chile: insights into the interplay between hydrothermal alteration and brittle deformation. J. Volcanol. Geotherm. Res. 324, 88–104.
Sánchez-Murillo, R., Aguirre-Dueñas, E., Gallardo-Amestica, M., Moya-Vega, P., Birkel, C., Esquivel-Hernández, G., Boll, J., 2018. Isotopic characterization of waters across Chile. Andean hydrology 1, 203–225.
Sepúlveda, F., Dorsch, K., Lahsen, A., Bender, S., Palacios, C., 2004. Chemical and isotopic composition of geothermal discharges from the Puyehue-Cordón Caulle area (40.5 S), Southern Chile. geothermics 33 (5), 655–673.
SERNAGEOMIN, 2019. Geo-parques Servicio Nacional de Geologia y Mineria, Chile. http://geachile.sernageomin.cl/.
Simmons, S.F., White, N.C., John, D.A., 2005. Geological characteristics of epithermal and base metal deposits. Economic Geology. 100th Anniversary Volume 485–522.
Slagter, S., Reich, M., Munoz-Saez, C., Southon, J., Morata, D., Barra, F., Gong, J., Skok, J.R., 2019. Environmental controls on silica sinter formation revealed by radiocarbon dating. Geology 47 (4), 330–334.
Spycher, N., Peiffer, L., Sonnenthal, E., 2013. GeoT user's guide a computer program for multicomponent geothermometry and geochemical speciation version 1.4. Lawrence Berkeley National Laboratory, Report No. LBNL-6172E.
Spycher, N., Peiffer, L., Sonnenthal, E.L., Saldi, G., Reed, M.H., Kennedy, B.M., 2014. Integrated multicomponent solute geothermometry. Geothermics 51, 113–123.
Stuiver, M., Polach, H.A., 1977. Reporting of C-14 data-discussion. Radiocarbon 19 (3), 355–363.
Stuiver, M., Reimer, P.J., 1993. Extended 14 C data base and revised CALIB 3.0 14 C age calibration program. Radiocarbon 35 (1), 215–230.
Tardani, D., Reich, M., Roulleau, E., Takahata, N., Sano, Y., Pérez-Flores, P., Sánchez-Alfaro, P., Cembrano, J., Arancibia, G., 2016. Exploring the structural controls on helium, nitrogen and carbon isotope signatures in hydrothermal fluids along an intra-arc fault system. Geochim. Cosmochim. Acta 184, 193–211.
Tassi, F., Aguilera, F., Darrah, T., Vaselli, O., Capaccioni, B., Poreda, R.J., Delgado Huertas, A., 2010. Fluid geochemistry of hydrothermal systems in the Arica-Parinacota, Tarapacá and Antofagasta regions (northern Chile). J. Volcanol. Geotherm. Res. 192, 1–15.
Vandemeulebrouck, J., Roux, P., Cros, E., 2013. The plumbing of Old Faithful Geyser revealed by hydrothermal tremor. Geophys. Res. Lett. 40 (10), 1989–1993.
Viles, H., Pentecost, A., 2007. Tufa and travertine. Geochemical Sediments and Landscapes, pp. 173–199.
Vogel, J.S., Southon, J.R., Nelson, D.E., Brown, T.A., 1984. Performance of catalytically condensed carbon for use in accelerator mass spectrometry. Nucl. Instrum. Methods Phys. Res., Sect. B 5 (2), 289–293.
Walter 1976.
Walter, T.R., Jousset, P., Allahbakhshi, M., Witt, T., Gudmundsson, M.T., Hersir, G.P., 2020. Underwater and drone based photogrammetry reveals structural control at Geysir geothermal field in Iceland. J. Volcanol. Geotherm. Res. 391, 106282.
Watts-Henwood, N., Campbell, K.A., Lynne, B.Y., Guido, D.M., Rowland, J.V., Browne, P.R., 2017. Snapshot of hot-spring sinter at Geyser Valley, Wairakei, New Zealand, following anthropogenic drawdown of the geothermal reservoir. Geothermics 68, 94–114.
Weir, G.J., Young, R.M., McGavin, P.N., 1992. A simple model for Geyser flat, Whakarewarewa. Geothermics 21 (1–2), 281–304.
Westall, F., de Wit, M.J., Dann, J., van der Gaast, S., de Ronde, C.E., Gerneke, D., 2001. Early Archean fossil bacteria and biofilms in hydrothermally-influenced sediments from the Barberton greenstone belt, South Africa. Precambrian Res. 106 (1–2), 93–116.
White, D.E., 1967. Some principles of geyser activity, mainly from Steamboat Springs, Nevada. Am. J. Sci. 265 (8), 641–684.
Wrage, J., Tardani, D., Reich, M., Daniele, L., Arancibia, G., Cembrano, J., Sánchez-Alfaro, P., Morata, D., Pérez-Moreno, R., 2017. Geochemistry of thermal waters in the Southern Volcanic Zone, Chile–Implications for structural controls on geothermal fluid composition. Chem. Geol. 466, 545–561.
Wu, S.M., Ward, K.M., Farrell, J., Lin, F.C., Karplus, M., Smith, R.B., 2017. Anatomy of Old Faithful from subsurface seismic imaging of the Yellowstone Upper Geyser Basin. Geophys. Res. Lett. 44 (20), 10–240.
Wu, S.M., Lin, F.C., Farrell, J., Allam, A., 2019. Imaging the deep subsurface plumbing of Old Faithful geyser from low-frequency hydrothermal tremor migration. Geophys. Res. Lett. 46 (13), 7315–7322.